

pubs.acs.org/macroletters Letter

Direct Observation of Micelle Fragmentation via In Situ Liquid-Phase Transmission Electron Microscopy

3 Julia T. Early, Kevin G. Yager, and Timothy P. Lodge*



Cite This: https://dx.doi.org/10.1021/acsmacrolett.0c00273



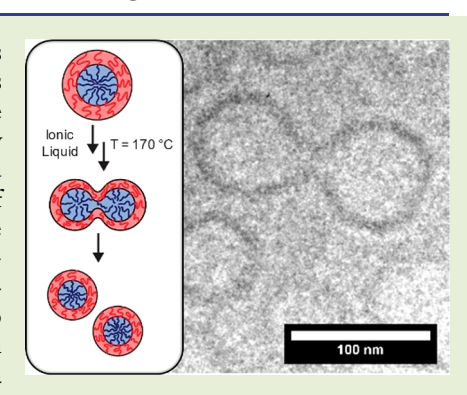
ACCESS

III Metrics & More

Article Recommendations

Supporting Information

4 ABSTRACT: Recently, attention has been directed toward understanding the dynamics and relaxation kinetics of block copolymer micelles, including mechanisms such as micelle fragmentation and fusion. The few prior studies on block copolymer micelle fragmentation relied on ensemble averaging techniques such as small-angle X-ray scattering and dynamic light scattering; some individual particles were imaged by ex situ transmission electron microscopy. Here we report the direct observation of fragmentation for three molecular weights of 1,2-polybutadiene-block-poly(ethylene oxide) (PB-PEO) micelles in the ionic liquid 1-ethyl-3-methylimidazolium bistic (trifluoromethylsulfonyl)imide using high-temperature liquid-phase transmission electron microscopy (LP-TEM). The use of in situ LP-TEM provides unique insights into the evolution of block copolymer micelles during fragmentation. Specifically, upon beating to 170 °C, a sequence of morphological transitions from a spherical micelle to a prolate ellipsoid, then a "peanut" shape, followed by a two-spherical-compartment micelle was observed, where the last is presumed to be the transition state.



-B diblock copolymers self-assemble into micelles of 19 Avarious morphologies when placed in a block-selective 20 solvent. These micelles are used in a range of applications such 21 as viscosity modification, oil recovery, and 22 drug or gene delivery. To fully realize the advantages of 23 block copolymer micelles in more complex applications, the 24 dynamics of micelle formation and equilibration should be 25 better understood. Significant progress toward quantifying 26 individual chain exchange kinetics has been reported for a 27 variety of block copolymers in selective solvents, including 28 organic solvents, water, and ionic liquids, where the micelle 29 size is close to or at equilibrium. 9-17 Yet, the equilibration 30 dynamics for block copolymer micelles that are kinetically 31 trapped at sizes far from equilibrium remain much less 32 understood. The mechanisms of fusion or fragmentation are 33 expected to contribute when the average micelle is, 34 respectively, either much smaller than or larger than the 35 equilibrium size. The mechanisms and kinetics of 36 equilibration for low molecular weight surfactants in aqueous 37 solutions have been studied extensively. 22-29 However, direct 38 experimental studies of block copolymer micelle fusion²¹ and 39 fragmentation 19,20,22,30,31 are rare.

Previous work by Meli et al. showed that direct dissolution (DD) of 1,2-polybutadiene-block-poly(ethylene oxide) (PB–42 PEO) diblock copolymers in the ionic liquid 1-ethyl-2-43 methylimidazolium bis(trifluoromethylsulfonyl)imide ([C_2MIM][TFSI]) resulted in kinetically trapped, large micelles. These micelles then became smaller, eventually reaching a steady state size, upon prolonged annealing at elevated temperatures. Similar evidence of fragmentation was

reported for PB-PEO micelles prepared by DD in various 1- 48 alkyl-3-methylimidazolium bis(trifluoromethylsulfonyl)imide- 49 based ionic liquids. 30,32,33 Although the as-prepared micelles 50 decreased in size when subjected to annealing at 170 °C, time- 51 resolved small-angle neutron scattering experiments revealed 52 that no individual chain exchange occurred under these 53 conditions.³⁰ Additionally, the kinetics of this process were 54 found to be independent of polymer concentration. Because 55 micelle fusion should be a second-order kinetic process with 56 respect to polymer concentration, 18,25,34 it was concluded that 57 PB-PEO micelles in these ionic liquids equilibrate primarily 58 by fragmentation.³⁰ This strong evidence for fragmentation 59 notwithstanding, the equilibration kinetics were determined 60 primarily by ensemble average methods such as dynamic light 61 scattering (DLS) and small-angle X-ray scattering (SAXS). 62 Direct imaging ex situ by transmission electron microscopy 63 (TEM) has also been employed.³³ Micelle fusion events have 64 recently been observed for aqueous polymer solutions using in 65 situ liquid cell transmission electron microscopy.²¹ To the best 66 of our knowledge, direct observation of fragmentation has not 67 been reported in any block copolymer/solvent system. Of 68 particular interest is the nature of the transition state.

Received: April 7, 2020 Accepted: May 4, 2020



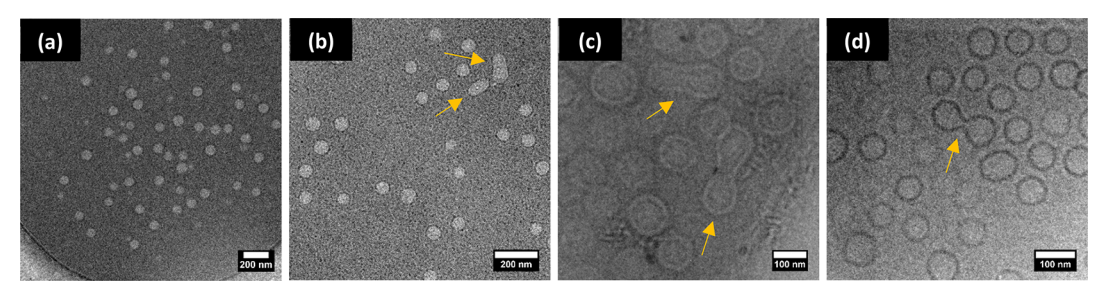


Figure 1. In situ LP-TEM images of 0.25 wt % BO(25–22) in $[C_2MIM][TFSI]$ annealing at T = 170 °C for (a) 2, (b) 20, (c) 180, and (d) 400 min. Orange arrows indicate micelles referenced in the text. The electron dose rate was 9.8 e⁻/Å² s at a magnification of 15000×.

In this work, we exploit the high thermal stability and nonvolatility of ionic liquids to conduct high-temperature liquid-phase TEM (LP-TEM) to observe in situ fragmentation of PB-PEO micelles in [C_2 MIM][TFSI]. Because the ionic liquid does not evaporate under the high vacuum conditions in the microscope, liquid samples can be imaged directly without the need for a hermetically sealed sample chamber. Using a temperature-controlled sample holder for LP-TEM allows T_1 jump experiments to be conducted directly in the microscope, and images of the change in the PB core morphology during fragmentation were collected. Additionally, time-resolved SAXS (TR-SAXS) experiments were performed to corroborate changes in the average core radius $\langle R_{\rm core} \rangle$ after a T_1 -jump to 170 s $^{\circ}$ C.

Three molecular weights of PB-PEO were synthesized by 85 two-step sequential anionic polymerization, as described ₈₆ previously, ³⁹ with a constant volume fraction of PEO, $f_{PEO} \cong$ 87 0.40.³⁹ PB-PEO diblocks and 0.1 wt % butylated hydrox-88 ytoluene as an antioxidant were dissolved in benzene and 89 freeze-dried under vacuum prior to use. Each molecular weight 90 of PB-PEO used in this work is referred to as BO(x-y), 91 where x and y denote the number-average molecular weight in 92 kDa (M_p) of the PB and PEO blocks, respectively. Size 93 exclusion chromatography with multiangle light scattering 94 detection showed that the three polymers studied, BO(8-7), 95 BO(25-22), and BO(27-27), had low dispersities ($\theta \leq$ 96 1.09); see Supporting Information for further molecular 97 characterization. Micelle solutions were prepared by the direct 98 dissolution (DD) method. The desired amounts of PB-PEO 99 and [C₂MIM][TFSI] were combined by weight in a 20 mL 100 scintillation vial equipped with a stir bar to obtain a 0.25 wt % solution. The vial was placed into an oil bath and stirred $_{102}$ vigorously at 70 $^{\circ}\text{C}$ for 48 h. The micelle core dimensions were 103 then studied in situ via high-temperature liquid-phase transmission electron microscopy (LP-TEM) and time-resolved 105 synchrotron small-angle X-ray scattering (TR-SAXS), as 106 discussed in the Supporting Information.

Prior to a *T*-jump to 170 °C, the PB core size for micelles as108 prepared by DD in $[C_2MIM][TFSI]$ was characterized by
109 room-temperature LP-TEM and SAXS. The initial average
110 core radius $(\langle R_{core} \rangle_0)$ for 0.25 wt % BO(8–7) in $[C_2MIM]$ 111 [TFSI] was found to be approximately 20 nm, with a standard
112 deviation $(\sigma_{core,0})$ of 6 nm by TEM image analysis. The 1D
113 scattering patterns for BO(8–7) by SAXS at room temperature
114 were fit to the Pedersen form factor for block copolymer
115 micelles with the Percus—Yevick structure factor. Hong the
116 fits, $(R_{core})_0 = 19.5 \pm 2.0$ nm for BO(8–7), in excellent
117 agreement with TEM. As shown in Figure S7, all micelles
118 observed for BO(8–7) by TEM were spherical. From Figure
119 S4, the form factor scattering for BO(8–7) micelles, as

prepared by DD and after a T-jump to 170 °C, are consistent 120 with a spherical core. The initial sizes of BO(25–22) and 121 BO(27–27) micelles in [C₂MIM][TFSI] were also deter- 122 mined in this manner and by TEM image analysis, $\langle R_{\rm core} \rangle_0 = 123$ 45 \pm 5 nm for BO(25–22) and $\langle R_{\rm core} \rangle_0 = 50 \pm 7$ nm for 124 BO(27–27). Again, the TEM images and SAXS data of these 125 samples in the Supporting Information confirm that the as- 126 prepared micelles are spherical.

As noted above, prior work on the equilibration kinetics of 128 PB-PEO in ionic liquids relied on ensemble average methods 129 to determine the evolution of micelle size during a T-jump, and 130 while the observed substantial decrease in the hydrodynamic 131 radius and core radius is consistent with fragmentation, this 132 phenomenon has yet to be observed in situ. 30,32,33 By 133 annealing the solutions directly in the electron microscope, a 134 series of images were obtained throughout the micelle 135 relaxation process, and the evolution of the core morphology 136 was monitored during fragmentation. Representative in situ 137 high-temperature LP-TEM images are shown in Figure 1 for 138 fl 0.25 wt % BO(25–22) in $[C_2MIM][TFSI]$ at 170 °C. Ideally, 139 the time evolution of individual micelles would be recorded 140 during annealing, but there are significant constraints on this 141 experiment. First, the characteristic equilibration times for the 142 polymers studied here are on the order of 10² to 10³ min, 143 making it difficult to track a single micelle in the TEM without 144 causing significant electron beam damage. Second, the particles 145 observed in LP-TEM are mobile and able to diffuse out of the 146 image frame throughout the experiment. Thus, while the time 147 series of images shown here are obtained for the same area of 148 the sample grid, it is difficult to establish how many micelles 149 remained within in the field of view throughout the annealing 150 process.

From Figure 1, the BO(25-22) micelle cores appear to be 152 spherical, yet the distribution of core radii is quite significant 153 after heating at 170 °C for 2 min (Figure 1a). After 20 min of 154 annealing, some micelles become distinctly elliptical, and the 155 core appears elongated compared to the image at 2 min; this is 156 presumably the first stage of fragmentation (Figure 1b). After 157 180 min of annealing, the elongated cores appear more like a 158 "peanut" with the formation of a shallow neck, which we 159 interpret as the second major morphological change to the 160 micelle structure during fragmentation (Figure 1c). After 161 annealing for 400 min at 170 °C, a finer neck is observed in 162 one micelle core undergoing fragmentation (Figure 1d). This 163 fine neck formation was the last anisotropic morphology 164 observed in BO(25-22) micelles during the experiment and is, 165 therefore, likely close to the final step in fragmentation, that is, 166 the transition state, before the complete separation of the core 167 into two smaller spherical micelles.

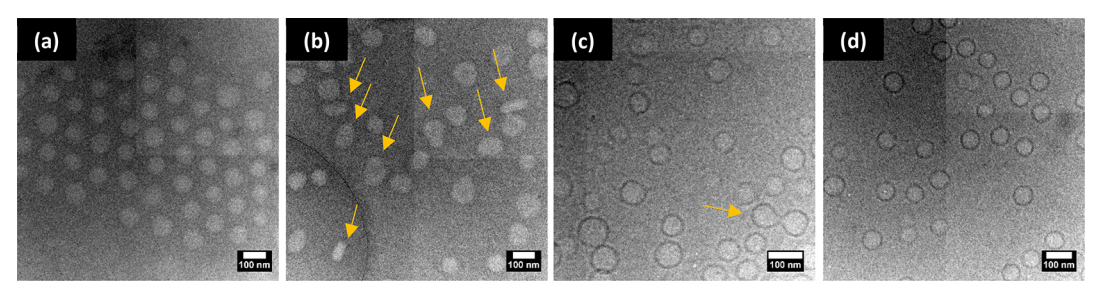


Figure 2. In situ LP-TEM images of 0.25 wt % BO(27–27) in $[C_2MIM][TFSI]$ annealing at T = 170 °C for (a) 5, (b) 45, (c) 320, and (d) 450 min. Orange arrows indicate micelles referenced in the text. The electron dose rate was 9.8 e⁻/Å² s at a magnification of 15000×.

Table 1. Automated Image Analysis of In Situ LP-TEM Images for 0.25 wt % PB-PEO in $[C_2MIM][TFSI]$ While Annealing at T = 170 °C

t (min)	$\langle R_{\rm core} \rangle^a (\rm nm)$	$\sigma_{\rm core}^{b}$ (nm)	Q^c	A^d (nm ²)	ε^e	$P \times R_{\text{core}}/A^f$	s_{core}^{g}
BO(8-7)							
5	20	2	1750	1230	0.5	2.1	2.2
20	18	2	1270	986	0.6	2.1	1.9
50	18	3	1340	1040	0.5	2.2	2.0
100	16	2	972	814	0.3	2.1	1.8
BO(25-22)							
2	43	9	6840	5700	0.4	2.1	2.9
20	35	11	3890	5180	0.6	2.5	2.4
180	33	8	3270	5780	0.5	2.7	2.3
400	30	5	2440	2930	0.1	2.1	2.0
BO(27-27)							
5	46	5	7520	6580	0.4	2.1	3.0
45	48	7	8720	7320	0.5	2.2	3.1
320	34	7	3000	3660	0.4	2.2	2.2
450	35	2	3450	3880	0.3	2.1	2.3

 $^a\langle R_{\rm core}\rangle = (A/\pi)^{1/2}$. One standard deviation from $\langle R_{\rm core}\rangle$. Aggregation number (Q) calculated as $4\pi\langle R_{\rm core}\rangle^3/(3V_{\rm PB})$, assuming the core is devoid of solvent, and $V_{\rm PB}$ is the volume per core chain. Surface area measured by automated image analysis. Eccentricity calculated by fitting an ellipse to the object, determined as $\varepsilon = (1-b^2/a^2)^{1/2}$; for a perfect circle, $\varepsilon = 0$, and for an infinitely long object, $\varepsilon = 1$. Perimeter × average radius/area is equal to 2 for a perfectly spherical boundary, and the boundary is less spherical if this value is greater than 2. $^gS_{\rm core}$ is the degree of core block stretching calculated as $\langle R_{\rm core}\rangle$ divided by the root-mean-square end-to-end distance of the core block.

As shown in Figure 2, a similar evolution of the core 169 170 morphology was observed for 0.25 wt % BO(27-27) in [C₂MIM][TFSI]. Note that the equilibration kinetics for this sample are slightly slower than for BO(25-22) micelles at 170 C and about an order of magnitude slower than for BO(8-7)micelles. A more quantitative study of the effect of molecular weight on fragmentation kinetics is currently in progress. The 176 PB core remains spherical after annealing at 170 °C for 5 min 177 (Figure 2a), but a variety of more elongated micelles emerge after annealing for 45 min (Figure 2b). It is interesting to note 179 the variety of anisotropic core morphologies observed in the 45 180 min image, and some particles appear to have formed a slight necking point. The fine-neck formation in one micelle was also observed for this sample after 320 min of annealing (Figure 183 2c), and after 450 min of annealing, the PB core morphology again appears spherical, but distinctly smaller (Figure 2d). The evolution of BO(8-7) micelles in [C₂MIM][TFSI] during annealing at 170 °C proceeds by the same general mechanism observed for BO(25-22) and BO(27-27) micelles, and in situ LP-TEM images for this polymer are shown in the Supporting Information, Figure S10.

190 It is important to address the contrast variation observed in 191 the in situ LP-TEM images. At short annealing times, the 192 micelle cores appear bright, with minimal appearance of 193 Fresnel fringes. During high-temperature annealing, the changes in sample height cause a variation of focus, which is 194 likely the cause for the appearance of darker Fresnel fringes at 195 longer times. This change in sample thickness is relatively 196 common in the LP-TEM literature, particularly for the open 197 environmental chamber used here. 36,42—44 Due to the short 198 lifetime of the fragmenting micelles, such as the one 199 highlighted in Figure 2c, focus adjustments were difficult to 200 perform. However, we conclude that this change in focus and 201 the appearance of dark Fresnel fringes in some of the images is 202 due to the experimental setup and not due to changes in the 203 mass distribution of the micelle core.

Additionally, the influence of beam damage on the micelle 205 structure is thought to be negligible compared to the effect of 206 the electron beam on the stability of the free-standing ionic 207 liquid films. 33,36 We observed that the ionic liquid films 208 become less stable at higher magnifications (>20000×) and at 209 elevated temperatures, where the formation of holes in the 210 liquid films becomes common. At higher temperatures and 211 magnification, the liquid layers can burst and adhere to the 212 holey carbon support. This phenomenon has been reported 213 previously for ionic liquids in an open environment LP-TEM, 36 214 and some examples of beam-damaged ionic liquid films are 215 provided in the Supporting Information.

To quantify the change in the core dimensions during 217 fragmentation, an automated image analysis routine was 218

219 applied to the images in Figures 1, 2, and S10 (details in the 220 Supporting Information). The count histograms generated by 221 the image analysis routine for the change in core radius and 222 area are shown in Figure S12 of the Supporting Information. 223 The average values obtained from image analysis are 224 summarized in Table 1. For each time point $\langle R_{\rm core} \rangle$ (nm), 225 $\sigma_{\rm core}$ (nm), mean aggregation number Q, core area A (nm²), 226 average eccentricity ε (where $\varepsilon=0$ for a perfectly spherical 227 object and ε approaches 1 for elongated, high aspect-ratio 228 objects), and $P \times R_{\rm core}/A$ were determined. $P \times R_{\rm core}/A$ is the 229 perimeter of the micelle core multiplied by the radius divided 230 by the area, which describes how circular the boundary of the 231 particle is if $P \times R_{\rm core}/A = 2$, then the boundary is perfectly 232 circular, and if $P \times R_{\rm core}/A > 2$, then the particle boundary has 233 more undulations.

From Table 1, $\langle R_{\text{core}} \rangle$ for all samples decreases with time, as 234 235 expected for micelle fragmentation. Interestingly, the ratio of 236 the aggregation numbers at the last to the first time points are $237 \, 0.55 \, \text{for BO}(8-7), \, 0.36 \, \text{for BO}(25-22), \, \text{and } 0.46 \, \text{for BO}(27-1), \, 0.36 \, \text{for BO}(25-22), \, 0.36 \, \text{for BO}(27-1), \, 0.36 \, \text{for BO}(25-22), \, 0.36 \, \text{for BO}(27-1), \, 0.36 \, \text{for BO}(25-22), \, 0.36 \, \text{for BO}(27-1), \, 0.36 \, \text{for BO}(25-22), \, 0.36 \, \text{for BO}(27-1), \, 0.36 \, \text{for BO}(25-22), \, 0.36 \, \text{for BO}(27-1), \, 0.36 \, \text{for BO}(25-22), \, 0.36 \, \text{for BO}(27-1), \, 0.36 \, \text{for BO}(25-22), \, 0.36 \, \text{for BO}(27-1), \, 0.36 \, \text{for BO}(27-1$ 238 27). This indicates that the BO(8-7) micelles after 100 min of annealing are approximately half of the size of the micelles after only 5 min of annealing. Similarly, BO(27-27) micelles contain approximately half of the number of polymer chains after 450 min of annealing compared to at only 5 min of 243 annealing. The decrease in Q for BO(25-22) is slightly more substantial, as the average number of chains per micelle decrease by almost 70% after 400 min of annealing compared 246 to 2 min of annealing at 170 °C. This decrease in Q for all samples further confirms that the micelles are equilibrating by 248 fragmentation. It also suggests that most, if not all, micelles 249 undergo only a single fragmentation event during these 250 experiments. This would be expected if the initial average 251 aggregation were approximately a factor of 2 larger than the 252 equilibrium value.

Another interesting trend is the change in the micelle 254 eccentricity ε throughout fragmentation. This was calculated 255 by fitting micelle images using the typical definition of 256 anisotropy for an ellipse. From Table 1, the average ε for all 257 micelles at the shortest annealing times is \sim 0.4–0.5, and the 258 eccentricity increases for intermediate annealing times, 259 consistent with the elongation of micelles during the early 260 stages of fragmentation. For the longest annealing times, the 261 eccentricity decreases to $\varepsilon \leq$ 0.3, which indicates the micelle 262 core achieves an even more spherical morphology after 263 fragmentation.

TR-SAXS at 170 °C was used to corroborate the change in $\langle R_{\rm core} \rangle$ with annealing time, where the background-subtracted 266 1D scattering intensity was fit to the Pedersen form factor 267 model for block copolymer micelles with the Percus-Yevick ²⁶⁸ hard sphere structure factor to directly obtain $\langle R_{\rm core} \rangle$ and $\sigma_{\rm core}$ ²⁶⁹ with superior temporal resolution and counting statistics than ²⁷⁰ LP-TEM. ^{40,41} The $\langle R_{\rm core} \rangle$ versus time from TR-SAXS for 0.25 271 wt % BO(8-7) in [C₂MIM][TFSI] and 0.25 wt % BO(27-272 27) in [C₂MIM][TFSI] are shown in Figure 3, superposed 273 with $\langle R_{\text{core}} \rangle$ determined by in situ LP-TEM from Table 1. 274 Longer annealing times are readily obtained with TR-SAXS, 275 and a steady-state $\langle R_{\text{core}} \rangle$ is reached, indicated by the second 276 plateau at longer t in Figure 3. For BO(8–7) micelles, $\langle R_{\text{core}} \rangle$ 277 values from TR-SAXS and LP-TEM agree remarkably well as a 278 function of time, which indicates that $\langle R_{\rm core} \rangle$ from the 279 automated TEM image analysis is consistent with the ensemble 280 average. This agreement is expected because the fragmentation time for BO(8-7) micelles is approximately 200 min, which is

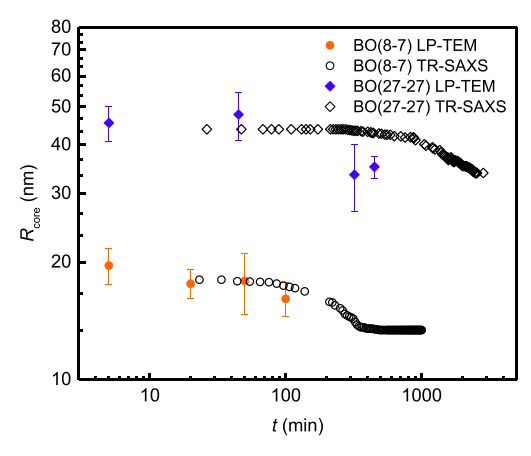


Figure 3. Image analysis of in situ LP-TEM of 0.25 wt % BO(8–7) (orange circles) and BO(27–27) (blue diamonds) in $[C_2MIM]$ -[TFSI] at 170 °C. The change in $\langle R_{\rm core} \rangle$ is determined using an automated image analysis program, where several micelles were measured for each time point. The error bars represent one standard deviation from the average value. Data points in black were determined by fitting the 1D scattering intensity obtained by TR-SAXS to the Pedersen model with the Percus–Yevick hard sphere structure factor.

a reasonable interval over which to conduct the LP-TEM 282 experiment. The $\langle R_{\rm core} \rangle$ obtained by each experiment for 283 BO(27–27) micelles agrees within the errors of the two 284 techniques at early times, but the $\langle R_{\rm core} \rangle$ values from LP-TEM 285 at 320 and 450 min are slightly smaller than the averages 286 obtained by TR-SAXS. As the number of micelles measured in 287 Figure 2 to obtain this average is relatively small (\sim 20–30 288 micelles), this is presumably not an adequate representation of 289 the ensemble $\langle R_{\rm core} \rangle$. Nevertheless, the kinetic information 290 from TR-SAXS supports the statistics obtained through 291 analysis of the LP-TEM images.

To rationalize the fragmentation kinetics reported previously 293 for BO(8-7) in ionic liquids 30,32,33 and to understand the 294 morphological evolution of the PB micelle core during 295 fragmentation observed here, we consider the degree of 296 chain stretching in the core (s_{core}) and the corona (s_{corona}) , 297 along with the extent of corona crowding in the transition state 298 for fragmentation. The proposed transition state of a "two- 299 spherical-compartment" micelle is illustrated in Figure 4 as 300 f4 structure IV. The equilibrium size and morphology of a micelle 301 is governed by the free energy balance among the core, corona, 302 and the interface. 45 The as-prepared micelles and those imaged 303 at the shortest annealing times exhibit a relatively high degree 304 of stretching in the core chains, as shown in Table 1, where 305 $s_{\rm core}$ was calculated as $\langle R_{\rm core} \rangle$ divided by the root-mean-square 306 end-to-end distance of the PB block. The relative stability of 307 the intermediates proposed in Figure 4 can explain the 308 observation of a small number of anisotropic micelles with a 309 neck for BO(25-22) and BO(27-27). It is likely that the 310 stability of the micelles illustrated in Figure 4 decreases as I > 311II > III > IV. Therefore, the number of micelles observed in 312 the experiment decreases in that order. Previous reports on the 313 fragmentation kinetics of BO(8-7) in $[C_2MIM][TFSI]$ found 314 that the change in $\langle R_{\text{core}} \rangle$ with annealing time is well described 315 by a compressed exponential with a compression exponent of 316 2.^{30,33} Although the mechanism of fragmentation was observed 317 here, the origin of the compressed exponential behavior 318 remains to be determined. The first stage of fragmentation 319 proceeds via the elongation of spherical micelles into a 320

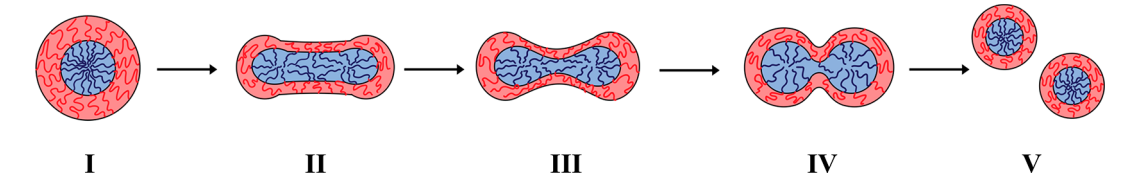


Figure 4. Schematic illustration of block copolymer micelle fragmentation, where the as-prepared micelles begin to elongate at short annealing times to relieve chain stretching in the larger, as-prepared micelles, followed by necking at longer annealing times and the thinning of the neck, which is believed to be the rate-limiting step to this process, and finally, separation of the micelle core and corona into two smaller micelles.

321 cylindrical morphology. This change in core area is entropically 322 favorable due to the relief of both core and corona chain stretching in the as-prepared micelles, but opposed by the 324 increased surface area. Previous measurements of fragmenta-325 tion in five different ionic liquids revealed that the kinetics 326 were largely independent of surface tension, indicating that the 327 transition state does not involve exposing the core to the solvent.³³ Rather, the kinetic barrier most likely results from 329 increased corona crowding during the neck formation in "twocompartment" micelles. In this scenario, the thinning of the 331 neck, represented as the fourth structure in Figure 4, causes 332 increased corona crowding for the polymer chains near the 333 necking point and is presumably close to the transition state. In summary, we report the direct observation of block 335 copolymer micelle fragmentation for PB-PEO in [C₂MIM]-336 [TFSI]. Due to the nonvolatility of ionic liquids, high-337 temperature LP-TEM allows imaging of dynamic processes 338 of soft matter in solution. From this work, we identified three 339 distinct changes in micelle core morphology during fragmen-340 tation. Initially, the micelles prepared by direct dissolution are 341 spherical, and upon heating to 170 °C, the micelles begin to 342 elongate. The elliptical micelles then begin to form a slight 343 neck, or peanut shape, and then the neck thins out to connect 344 two nearly spherical core compartments, which we hypothesize 345 is the rate limiting step in micelle fragmentation; further 346 annealing results in the necked micelles to fragment into two 347 smaller micelles.

ASSOCIATED CONTENT

Supporting Information

352

353

356

357

358

359

360

361

362

363

364

365

366

367

368

350 The Supporting Information is available free of charge at 351 https://pubs.acs.org/doi/10.1021/acsmacrolett.0c00273.

> Synthesis and characterization of BO(8-7), BO(25-22), BO(27–27), and $[C_2MIM][TFSI]$, SEC-RI trace of BO polymers in THF, ¹H NMR spectra of BO polymers and [C₂MIM][TFSI], experimental details for in situ and ex situ LP-TEM and SAXS, background subtracted SAXS profiles of 0.25 wt % BO(8-7), BO(25-22), and BO(27-27) micelles in [C₂MIM][TFSI], ex situ LP-TEM images of 0.25 wt % BO(8-7), BO(25-22), and BO(27-27) in [C₂MIM][TFSI], as prepared by DD and steady-state after a T-jump to 170 °C, in situ LP-TEM images of 0.25 wt % BO(8-7) in $[C_2MIM][TFSI]$ at T = 170 °C, automated image analysis results for 0.25 wt % BO(27-27) in $[C_2MIM][TFSI]$, experimental details for dynamic light scattering, and dynamic light scattering of 0.25 wt % BO(27–27) in $[C_2MIM][TFSI]$, as prepared by DD and steady-state after a T-jump to 170 °C (PDF)

AUTHOR INFORMATION

Corresponding Author

Timothy P. Lodge – Department of Chemistry and Department 371 of Chemical Engineering and Materials Science, University of Minnesota, Minneapolis, Minnesota 55455-0431, United States; o orcid.org/0000-0001-5916-8834; Email: lodge@ umn.edu

369

370

373

374

375

382

383

384

385

386

408

Authors 376

Julia T. Early - Department of Chemistry, University of 377 Minnesota, Minneapolis, Minnesota 55455-0431, United States 378 Kevin G. Yager – Center for Functional Nanomaterials, 379 Brookhaven National Laboratory, Upton, New York 11973, 380 *United States;* © orcid.org/0000-0001-7745-2513 381

Complete contact information is available at: https://pubs.acs.org/10.1021/acsmacrolett.0c00273

Notes

The authors declare no competing financial interest.

ACKNOWLEDGMENTS

This work was supported primarily by the National Science 387 Foundation (DMR-1707578) and by the U.S. Department of 388 Energy (DOE), Office of Science, Office of Workforce 389 Development for Teachers and Scientists, Office of Science 390 Graduate Student Research (SCGSR) program. The SCGSR 391 program is administered by the Oak Ridge Institute for Science 392 and Education (ORISE) for the DOE. ORISE is managed by 393 ORAU under Contract No. DE-SC0014664. Portions of this 394 work were performed at the Center for Functional Nanoma- 395 terials, and the National Synchrotron Light Source II, 396 Brookhaven National Laboratory, which are supported by 397 the U.S. DOE Office of Science under Contract No. DE- 398 SC0012704. Data were collected using an instrument funded 399 by the National Science Foundation under Award No. 400 0960140. Parts of this work were carried out in the 401 Characterization Facility, University of Minnesota, which 402 receives partial support from NSF through the MRSEC 403 program (DMR-1420013). We thank Dr. Ruipeng Li and Dr. 404 Esther Tsai for assistance with TR-SAXS measurements at the 405 11-BM CMS beamline at the NSLS-II and Dr. Lihua Zhang for 406 insightful discussions on high temperature LP-TEM.

REFERENCES

- (1) Anderson, W. Block Copolymers as Viscosity Index Improvers for 409 Lubrication Oils; 1973, 3763044.
- (2) Raffa, P.; Broekhuis, A. A.; Picchioni, F. Polymeric Surfactants 411 for Enhanced Oil Recovery: A Review. J. Pet. Sci. Eng. 2016, 145, 412
- (3) Wever, D. A. Z.; Picchioni, F.; Broekhuis, A. A. Polymers for 414 Enhanced Oil Recovery: A Paradigm for Structure-Property Relation- 415 ship in Aqueous Solution. Prog. Polym. Sci. 2011, 36, 1558-1628.

- 417 (4) Pavía-Sanders, A.; Zhang, S.; Flores, J. A.; Sanders, J. E.; 418 Raymond, J. E.; Wooley, K. L. Robust Magnetic/Polymer Hybrid 419 Nanoparticles Designed for Crude Oil Entrapment and Recovery in 420 Aqueous Environments. *ACS Nano* **2013**, *7*, 7552–7561.
- 421 (5) Cotanda, P.; Lu, A.; Patterson, J. P.; Petzetakis, N.; O'Reilly, R. 422 K. Functionalized Organocatalytic Nanoreactors: Hydrophobic 423 Pockets for Acylation Reactions in Water. *Macromolecules* **2012**, *45*, 424 2377–2384.
- 425 (6) Tyrrell, Z. L.; Shen, Y.; Radosz, M. Fabrication of Micellar 426 Nanoparticles for Drug Delivery through the Self-Assembly of Block 427 Copolymers. *Prog. Polym. Sci.* **2010**, *35*, 1128–1143.
- 428 (7) Hubbell, J. A. Enhancing Drug Function. Science (Washington, 429 DC, U. S.) 2003, 300, 595-596.
- 430 (8) Meier, W. Polymer Nanocapsules. *Chem. Soc. Rev.* **2000**, 29, 431 295–303.
- 432 (9) Zhao, D.; Ma, Y.; Lodge, T. P. Exchange Kinetics for a Single 433 Block Copolymer in Micelles of Two Different Sizes. *Macromolecules* 434 **2018**, *51*, 2312–2320.
- 435 (10) Zinn, T.; Willner, L.; Pipich, V.; Richter, D.; Lund, R. 436 Molecular Exchange Kinetics of Micelles: Corona Chain Length 437 Dependence. ACS Macro Lett. 2016, 5, 884–888.
- 438 ($\bar{1}$ 1) Ma, Y.; Lodge, T. P. Chain Exchange Kinetics in Diblock 439 Copolymer Micelles in Ionic Liquids: The Role of χ . *Macromolecules* 440 **2016**, 49, 9542–9552.
- 441 (12) Willner, L.; Poppe, A.; Allgaier, J.; Monkenbusch, M.; Richter, 442 D. Time-Resolved SANS for the Determination of Unimer Exchange 443 Kinetics in Block Copolymer Micelles. *Europhys. Lett.* **2001**, *55*, 667–444 673.
- 445 (13) Lund, R.; Willner, L.; Stellbrink, J.; Lindner, P.; Richter, D. 446 Logarithmic Chain-Exchange Kinetics of Diblock Copolymer 447 Micelles. *Phys. Rev. Lett.* **2006**, *96*, 1–4.
- 448 (14) Lund, R.; Willner, L.; Richter, D.; Dormidontova, E. E. 449 Equilibrium Chain Exchange Kinetics of Diblock Copolymer Micelles: 450 Tuning and Logarithmic Relaxation. *Macromolecules* **2006**, 39, 4566–451 4575.
- 452 (15) Choi, S. H.; Lodge, T. P.; Bates, F. S. Mechanism of Molecular 453 Exchange in Diblock Copolymer Micelles: Hypersensitivity to Core 454 Chain Length. *Phys. Rev. Lett.* **2010**, *104*, 1–4.
- 455 (16) Lu, J.; Bates, F. S.; Lodge, T. P. Chain Exchange in Binary 456 Copolymer Micelles at Equilibrium: Confirmation of the Independent 457 Chain Hypothesis. *ACS Macro Lett.* **2013**, *2*, 451–455.
- 458 (17) Wang, E.; Lu, J.; Bates, F. S.; Lodge, T. P. Effect of Corona 459 Block Length on the Structure and Chain Exchange Kinetics of Block 460 Copolymer Micelles. *Macromolecules* **2018**, *51*, 3563–3571.
- 461 (18) Dormidontova, E. E. Micellization Kinetics in Block Copolymer 462 Solutions: Scaling Model. *Macromolecules* **1999**, 32, 7630–7644.
- 463 (19) Rharbi, Y. Fusion and Fragmentation Dynamics at Equilibrium 464 in Triblock Copolymer Micelles. *Macromolecules* **2012**, 45, 9823–465 9826.
- 466 (20) Rharbi, Y.; Karrouch, M.; Richardson, P. Fusion and Fission 467 Inhibited by the Same Mechanism in Electrostatically Charged 468 Surfactant Micelles. *Langmuir* **2014**, *30*, 7947–7952.
- 469 (21) Parent, L. R.; Bakalis, E.; Ramírez-Hernández, A.; Kammeyer, J. 470 K.; Park, C.; De Pablo, J.; Zerbetto, F.; Patterson, J. P.; Gianneschi, N. 471 C. Directly Observing Micelle Fusion and Growth in Solution by 472 Liquid-Cell Transmission Electron Microscopy. *J. Am. Chem. Soc.* 473 **2017**, 139, 17140–17151.
- 474 (22) Rharbi, Y.; Li, M.; Winnik, M. A.; Hahn, K. G. Temperature 475 Dependence of Fusion and Fragmentation Kinetics of Triton X-100 476 Micelles. *J. Am. Chem. Soc.* **2000**, *122*, *6242–6251*.
- 477 (23) Rharbi, Y.; Winnik, M. A. Salt Effects on Solute Exchange and 478 Micelle Fission in Sodium Dodecyl Sulfate Micelles below the 479 Micelle-to-Rod Transition. *J. Phys. Chem. B* **2003**, *107*, 1491–1501.
- 480 (24) Rharbi, Y.; Kitaev, V.; Winnik, M. A.; Hahn, K. G. 481 Characterizing Aqueous Micellar Triton X-100 Solutions of a
- 482 Fluorescent Model Triglyceride. *Langmuir* **1999**, *15*, 2259–2266.
 483 (25) Rharbi, Y.; Winnik, M. A.; Hahn, K. G. Kinetics of Fusion and
 484 Fragmentation Nonionic Micelles: Triton X-100. *Langmuir* **1999**, *15*,

485 4697-4700.

- (26) Rharbi, Y.; Winnik, M. A. Salt Effects on Solute Exchange in 486 Sodium Dodecyl Sulfate Micelles. *J. Am. Chem. Soc.* **2002**, 124, 2082—487 2083 see Chart 1: (a) Exchange via Water Mechanism, (b) Collision-488 Exchange-Separation Mechanism, and (c) Fragmentation-Growth 489 Mechanism.
- (27) Aniansson, E. A. G.; Wall, S. N.; Almgren, M.; Hoffmann, H.; 491 Kielmann, I.; Ulbricht, W.; Zana, R.; Lang, J.; Tondre, C. Theory of 492 the Kinetics of Micellar Equilibria and Quantitative Interpretation of 493 Chemical Relaxation Studies of Micellar Solutions of Ionic 494 Surfactants. *J. Phys. Chem.* **1976**, 80, 905–922.
- (28) Zana, R. Dynamics in Micellar Solutions of Amphiphilic Block 496 Copolymers. In *Dynamics of Surfactant Self-Assemblies: Micelles, 497 Microemulsions, Vesicles, and Lyotropic Phases*; Hubbard, A. T., Ed.; 498 Taylor & Francis Group/CRC Press: Boca Raton, FL, 2005; pp 161–499 231.
- (29) Michels, B.; Waton, G.; Zana, R. Dynamics of Micelles of 501 Poly(ethylene oxide)—Poly(propylene oxide)—Poly(ethylene oxide) 502 Block Copolymers in Aqueous Solutions. *Langmuir* **1997**, *13*, 3111—503 3118.
- (30) Meli, L.; Santiago, J. M.; Lodge, T. P. Path-Dependent 505 Morphology and Relaxation Kinetics of Highly Amphiphilic Diblock 506 Copolymer Micelles in Ionic Liquids. *Macromolecules* **2010**, 43, 507 2018–2027.
- (31) Zakharov, A. I.; Adzhemyan, L. T.; Shchekin, A. K. Relaxation 509 Times and Modes of Disturbed Aggregate Distribution in Micellar 510 Solutions with Fusion and Fission of Micelles. *J. Chem. Phys.* **2015**, 511 143, 124902.
- (32) Meli, L.; Lodge, T. P. Equilibrium vs Metastability: High- 513 Temperature Annealing of Spherical Block Copolymer Micelles in an 514 Ionic Liquid. *Macromolecules* **2009**, 42, 580–583.
- (33) Early, J. T.; Lodge, T. P. Fragmentation of 1,2-Polybutadiene- 516 Block-Poly(Ethylene Oxide) Micelles in Imidazolium-Based Ionic 517 Liquids. *Macromolecules* **2019**, 52, 7089–7101.
- (34) Halperin, A.; Alexander, S. Polymeric Micelles: Their 519 Relaxation Kinetics. *Macromolecules* **1989**, 22, 2403–2412.
- (35) Kim, P. Y.; Ribbe, A. E.; Russell, T. P.; Hoagland, D. A. 521 Visualizing the Dynamics of Nanoparticles in Liquids by Scanning 522 Electron Microscopy. ACS Nano 2016, 10, 6257–6264.
- (36) Mansfeld, U.; Hoeppener, S.; Schubert, U. S. Investigating the 524 Motion of Diblock Copolymer Assemblies in Ionic Liquids by in Situ 525 Electron Microscopy. *Adv. Mater.* **2013**, *25*, 761–765.
- (37) Kuwabata, S.; Tsuda, T.; Torimoto, T. Room-Temperature 527 Ionic Liquid. A New Medium for Material Production and Analyses 528 under Vacuum Conditions. *J. Phys. Chem. Lett.* **2010**, *1*, 3177–3188. 529
- (38) Uematsu, T.; Baba, M.; Oshima, Y.; Tsuda, T.; Torimoto, T.; 530 Kuwabata, S. Atomic Resolution Imaging of Gold Nanoparticle 531 Generation and Growth in Ionic Liquids. *J. Am. Chem. Soc.* **2014**, *136*, 532 13789–13797.
- (39) Hillmyer, M. A.; Bates, F. S. Synthesis and Characterization of 534 Model Polyalkane-Poly(Ethylene Oxide) Block Copolymers. *Macro-* 535 *molecules* **1996**, 29, 6994–7002.
- (40) Pedersen, J. S.; Svaneborg, C.; Almdal, K.; Hamley, I. W.; 537 Young, R. N. A Small-Angle Neutron and x-Ray Contrast Variation 538 Scattering Study of the Structure of Block Copolymer Micelles: 539 Corona Shape and Excluded Volume Interactions. *Macromolecules* 540 **2003**, 36, 416–433.
- (41) Pedersen, J. S. Determination of Size Distributions from Small- 542 Angle Scattering Data for Systems with Effective Hard-Sphere 543 Interactions. J. Appl. Crystallogr. 1994, 27, 595–608.
- (42) De Jonge, N.; Ross, F. M. Electron Microscopy of Specimens in 548 Liquid. Nat. Nanotechnol. 2011, 6, 695–704.
- (43) Helveg, S.; López-Cartes, C.; Sehested, J.; Hansen, P. L.; 547 Clausen, B. S.; Rostrup-Nielsen, J. R.; Abild-Pedersen, F.; Nørskov, J. 548 K. Atomic-Scale Imaging of Carbon Nanofibre Growth. *Nature* **2004**, 549 427, 426–429.
- (44) Dai, L. L.; Sharma, R.; Wu, C. Y. Self-Assembled Structure of 551 Nanoparticles at a Liquid-Liquid Interface. *Langmuir* **2005**, *21*, 2641–552 2643.

554 (45) Zhulina, E. B.; Adam, M.; Larue, I.; Sheiko, S. S.; Rubinstein, 555 M. Diblock Copolymer Micelles in a Dilute Solution. *Macromolecules* 556 **2005**, 38, 5330–5351.